Drones in turbulence

Roosenburg, Jori J.

Award date:
2019

Bachelor thesis

Drones in turbulence

Bachelor Thesis by

J.J. Roosenburg

Supervisor:

F. Toschi

25/09/2019

R-1994-B

For the department of physics technical university of Eindhoven.
Turbulence and vortex dynamics group.

Abstract.

In order to understand if a drone can measure turbulence an effort is made to modify the flight controller of an existing drone to experiment with. In this report a section is dedicated to control theory and the implementation on the drone, though this is not the main focus of the work. A part of the paper is dedicated to the 3d localization of the drone using a Kinect sensor to compensate for drifting, though due to technical limitations the drone has been suspended and has been used as a large particle to measure turbulence. Using this method we could correlate the signal from the accelerometer with the statistical properties of the turbulent flow profile. This may possible allow relating accelerometer data to its turbulent fluctuations.

Table of Contents

1 Introduction

Flying drones has been a pastime expenditure rising in popularity. In recent years the manufacturing costs of drones have been decreasing and therefore these could become a low cost measuring solution. A field of research that could use such application is turbulence. Can we use a drone to research turbulence? What are the minimum required specifications on a drone to obtain a required level of precision? Turbulence has been studied for larger aircraft, but for drones, turbulence may be even more important due to the size of the drones and its propellers behavior. Even so drones in turbulence have not been extensively studied. With regard to measuring turbulence, drones add the proposition of being able to measure on different size scales and are also applicable in otherwise difficult to reach places such as turbulent air layers. Furthermore using a drone in a turbulence environment using AI might be used in order to increase the performance of its flight controller and increase its efficiency. Therefore using a drone to measure turbulence has multiple application and thus great promise.

1.1 Outline of this thesis

This thesis is meant to show what steps are used in order to make a drone do measurements on turbulence. What steps are taken and why. The reader is also provided, in each chapter, with some basic theory to support the discussion on the methods and findings.

Chapter 2 discusses the basics of turbulence required for this work. Some understanding of fluid dynamics is required, but an attempt is made to make this chapter readable for a broader audience. The fundamentals of this chapter will assist in understanding the complete thesis. In chapter 3 the drone will be discussed in all its assets as it is a crucial part of this thesis. Making a drone fly is not a trivial task, flying it in turbulence even les. Therefore understanding its fundamentals is very important. The technical details, its control system and its shortcomings such as its sensors will be discussed in this section. Which leads to chapter 4: the image acquisition. This chapter is all about the secondary system to validate and to assist the drone in its measurement. In a preferred scenario the drone is fully independent but this goal has not been achieved yet in this project. The image acquisition itself is made from scratch and its design and function will be discussed here. Which leads to actual testing in chapter 5, here light will be shed on the probability distribution functions of the sub-systems and thereafter on turbulence itself. This is the chapter containing main results of the thesis. Conclusions follow in chapter 6.

2 Turbulence

2.1 Introduction/history

The first known attempt of modeling turbulence dates back to drawings from Leonardo da Vinci, relating it to the unpredictable ways of movement in nature [1]. Turbulence holds a special place in physics for this reason, it could be stated that it is the first example challenging the thoughts on determinacy and introducing chaos.

Turbulence is chaotic, to a level where even short term solutions are not possible to be predicted. Due to the closure problem, solving for the evolution of statistical moments of the velocity fields leads to more unknowns than equations, making the solution of turbulence equation impossible for a long period of time. In modern days, direct numerical simulations (DNS) can be used to solve turbulence in a quantitive manner. Although these numerical methods are very useful they do not help towards a more fundamental solution for turbulence [2]. Due to its limited scope of this thesis it shall focus only on the basics needed to explain the works results.

2.2 Fundamentals

Looking at turbulence, its fluctuations and its behavior look chaotic that it may appear to be random, even if, being turbulence a solution of the Navier-Stokes equation, it is therefore deterministic [3]. Accepting chaotic the nature of turbulence scientists have tried to understand it using statistical tools.

Turbulence occurs as a result of instability in a stable flow profile. When the shear within a flow becomes too high, instabilities occur as shown in [figure 2.1].

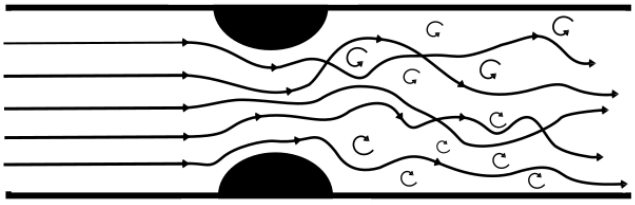

FIGURE 2.1: IMPRESSION OF HOW TURBULENCE DEVELOPS IN A TUBE DUE TO AN OBSTACLE IN THE TUBE .

This results in the formation of unstable eddies are considered the fundamental entities in turbulent flow, big eddies cascade to form smaller eddies, until a scale is reached where energy is dissipated due to viscosity, turning kinetic energy into heat.

Based on the fundamentals of this phenomenological theory, Kolmogorov postulated that for high enough Reynolds number the smallest eddies are independent of the geometry and therefore statistically isotropic (Kolmogorov's hypothesis of local isotropy). On the smallest scale all energy should be dissipated, based on the energy dissipation ε and on the kinematic viscosity ν. The Kolmogorov scales for length, time and speed (2.1, 2.2, 2.3) given by:

$$\eta = \left(\frac{\nu^3}{\varepsilon}\right)^{1/4}, \tau = \left(\frac{\nu}{\varepsilon}\right)^{1/2}, u = (\nu\varepsilon)^{1/2}. \qquad (2.1,2.2,3.3)$$

The Kolmogorov scales characterize the minimum dimensions of eddies in turbulence. At larger length scales viscous terms are negligible. An expression for kinetic energy over different eddy sizes is given by denoted as the -5/3rd equation (2.4), is a good approximation to experimental observed behavior. The constant C by experimentation found to be close to 1.5 [3]:

$$E(k) = C\frac{\varepsilon^{2/3}}{k^{5/2}}. \qquad (2.4)$$

2.3 Acceleration in turbulence

The primary tool of measurement is the accelerometer, therefore the statistical behavior of acceleration in turbulence is of upmost interest. A unique feature of drones is that they are capable of measurements in the Lagrangian frame of reference. Acceleration and velocities can be related to the flow Reynolds number and therefore to its level of turbulence. Using the typical length scales of the flow its velocity and the dimensions of the drone its level of turbulence can be estimated.

2.4 Stirring turbulence

In nature turbulence is ubiquitous for examples behind rocks in a flowing river. While this is a very basic example of turbulence, this simple principle inspires the passive grid method for generating turbulence as used in wind tunnels. By adding a grid to a laminar flow allows developing an almost isotropic and homogeneous turbulent flow. This type of turbulence is limited by the dimensions of the grid and of the wind tunnel to low Reynold numbers. A more interesting way of creating turbulence is using an active grid, it uses stepping motors and vanes attached on bars performing a random motion as driven by an algorithm. This allows to create a stronger level of turbulence than a passive grid would allow. This methods gives in slightly on isotropy compared to the passive grid [5].

3 Quadcopter Drone

3.1 Quadcopter - Drone physics

In recent year's quadcopter are in such demand that laws have been made to restrict usage in certain areas showing its popularity among consumers. But the research on drones is still ongoing and in the last few years, a multitude of papers were published on flying and optimization of drones [7]. Is of great importance to know how a drone functions. Following the work of the Control Systems Technology Group at the Technical University Eindhoven (TU/e).

3.1.1 Physical Model

In this model the quadcopter is modeled as a rigid body with [figure 3.1] depicting its free body diagram. Where the frame of reference is Eulerian with its z axis corresponding to gravity. Each rotor is able to give its unique thrust to its rotation speed [7], also each propeller gives a unique torque which is the reason for its orientation. A complete mathematical model is noted in [10] which we are not going to reproduce since it is falls out of the focus of this chapter. One should understand how the thrust on each individual rotor can influence its orientation, or rather how its relative speed of rotors governs its attitude. This relationship, looking at [figure 3.1], is rather simple: when rotors 1 and 4 increase their speed compared to rotors 2 and 3, the drone will roll in its positive direction. This holds true for each angle giving the model a way to change orientation. A bit less intuitive is its rotation about its z axis which requires use of torque increasing the relative speed of 1 and 3 to 2 and 4.

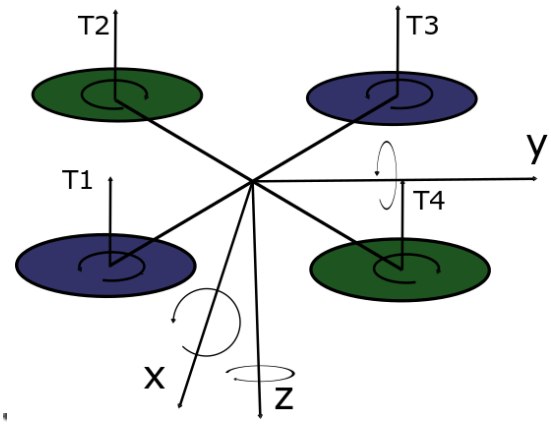

FIGURE 3.1 FREE BODY DIAGRAM OF QUADCOPTER THE DRONE. WITH INVERTED ITS PRINCIPAL AXIS AND ITS ROTATIONAL AXIS.

3.2 Drone Specification

When looking for a drone there are a multitude of choices. Research drones have to qualify for specific criteria, they needs to be fully programmable. Also size is a requirement, for the dimensions of the wind tunnel and therefore the area of flight. Also turbulence has a different effect on different length scales and therefore the size matters. Lastly the quality of its sensors play a critical role in how well it is able to fly and measure. Based on these criteria the Parrot mambo mini [11] was chosen. For its relative size but mostly for the multitude of ways to interact with the drone, specifications in table 3.1. The Parrot mambo uses a Bluetooth protocol, and therefore can be used by any computer using the right Bluetooth adapter. Sequentially Matlab/Simulink are supported which can be a downside but an upside as well due to personal preference. Using Simulink's add on for the Parrot mambo making an integral part of building a flight controller easier, but leaving some full control. The Simulink program compiles the flight controller to C code and uploads it to the drone, so the drone essentially flights on C-code. Alternatively the drone can also be programmed from a SDK method.

Width: 180 mm
Length: 180 mm
Weight: 63 gram
Ultrasound
Barometer
3 axis accelerometer
3 axis gyroscope

TABLE 3.1 MECHANICAL PROPERTIES OF THE DRONE.

3.3 Flight Controller

A drone is inherently unstable because it has only 4 actuators and 6 degrees of freedom. Therefore a differential control system is needed to compensate for this instability. Many solutions to flight controllers for quadcopters have been made but applying one to a new system is not trivial. The drone is made to fly by itself using a closed loop PID controller using cascade control [7]. The system is reliant on 2 separate state estimations both individually for its attitude and altitude.

3.3.1 Control theory

Control theory allows to operate continuously dynamic systems, with different goals; for this thesis we focus on reaching a certain state. This is done by using a closed loop system according to [figure 3.2]. The system has an input about its environment and its current situation, based on these values the system takes action in order to reach another state, hopefully reaching the reference state. For example: when the drone would be tilted in with respect to the reference state, it would take action in order to reduce the difference. This can be done using 3 separate techniques, its proportional controller, the differential controller or its integral controller therefore it is called a PID controller, for reference and further reading [7].

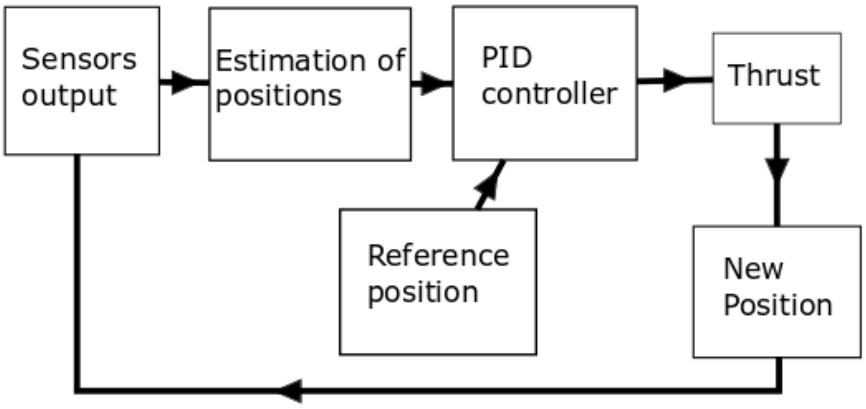

FIGURE 3.2 SIMPLIFIED INFORMATIVE GRAPH DEPICTING THE PID CLOSED LOOP SYSTEM

Proportional

Proportional is the simplest and most intuitive method of control. When there is a difference between its reference value and its current value it acts based on its difference. For some systems using only this controller is sufficient, usually this applies to systems that are stable and slow (an example would be a thermostat) but the drone is an unstable system and therefore the Proportional controller is not sufficient on its own.

Differential

The differential controller uses more than just his current state, it uses previous information to make a prediction not only on its change but also on its rate of

change. This is to mitigate the effect of overshooting its reference value, using the derivative of the error term to take action.

Integral

The integral controller is the less used controller, its effect is best seen on the long term behavior reducing its steady state error, which is the error between the long term desired state and the state the system stabilizes at. The deviation from the desired stat is not preferred and the integral term helps reducing/removing the steady state error.

These terms are expressing in the form of a function according to formula (8) where each term has its own balancing term to balance each effect. This is the formula in the state space where it is not governed by time anymore but work in the state domain sufficing to both continuous and discrete systems.

$$u(s) = K_P e(s) + K_I \frac{1}{s} e(s) + K_D s e(s). \quad (8)$$

3.4 State estimation

The drone itself has limited sensors, which means that not all state information is known, but with use of the sensors its position can be estimated. Here the quality and method of such estimate is discussed.

3.4.1 Attitude

The individual axis are all using their own PID controller, pitch yaw and roll. Therefore for each of these axis the state has to be calculated. The pitch and roll can be determined using gravity, but the yaw is best measured using a magnetometer using earth's magnetic field to orient.

Pitch and yaw are essentially the same but on tangent directions. Using the accelerometer combined with some geometry an estimate can be made on its attitude using formulas (9, 10);

$$\varphi = ArcTan\left(\frac{a_y}{a_z}\right), \theta = ArcTan\left(\frac{\sqrt{{a_x}^2 + {a_z}^2}}{a_y}\right). \quad (9, 10)$$

This estimate is not perfect on itself, external forces will create errors in this estimation, therefore the gyroscope information is used to compensate this effect. Integrating the angular acceleration gives a speed and therefore a rate of change of its angles. This signal has drift due to the integration, creating an estimator losing precision over time. Using a complementary filter these estimates can be combined to balance out the fundamental issues of these estimators. The complementary filter adds the findings of both estimates and levels them out using the previous angle for the gyroscope estimation.

3.4.2 Altitude

Determining the altitude can be done in multiple ways, an ultrasonic sensor has its advantages but it is mostly used for landing due to its short range. Therefore the pressure sensor was used in earlier stages, something not very feasible in turbulence. The accelerometer is used in the same sense the gyroscope is used in attitude estimation. Its integration finds a speed in a certain direction which can be used for its altitude. This works but suffers from drift. Due to the pressure differences a visual sensor is needed. The camera on the drone requires too much processing power on the drone and it is not supported at the time of this work, therefore external localization will be used to determine the drones altitude. Combining both the acceleration and the image acquisition in a Kalman filter to optimize its estimation.

3.5 Communication

Signals are sent using the UDP protocol over Bluetooth 4.0 using a CSR 4.0 adapter. The drone has the ability to fly manually or automatic. The controller is running on the chip of the drone. While flying, the drone is able to send the data from its sensor for analytics and receiving data from the Kinect regarding its position. The sampling of sending and receiving has to be limited to prevent an overflow of data on the drone, this limit is ~10 times lower than its processing speed.

4 Image Acquisition

In order to receive extra information about the drone a Kinect system is used as a reference measurement. It is a Kinect v2 used on a Windows computer, using the Matlab© support package for image acquisition. This enables for both a reference measurement and additional input for the drones flight system.

4.1 Kinect v2

The Kinect v2 uses time of flight technology to determine depth. The time of flight principle sends out infrared, using his camera, all 3d information can be found without modifying the drone and can therefore be used on any type of drone.

FIGURE 4.1 AN ENHANCED BACKGROUND IMAGE OF THE WINDTUNNEL MADE WITH THE KINECT DEPTH SENSOR.

4.2 Applying the data

The Kinect output shows a 2d picture using pixel color as depth information a typical image looking like Fig. 4.1 using a static position without the drone in place its background can be filtered out and, therefore, only the foreground will remain seen. When no drone is present this would result in a fully black image. The filter is made using a background measurement of ~60 seconds. The video data can be represented by figure 4.2. Treating each pixel position as a row over time its values follow a normal distribution as seen in Fig. 4.3. Using an inverse cumulative distribution function (4.1) containing both the mean and standard deviation of the pixel row but also an intended precision in P and its inverse error function:

$$\mu + \sqrt{2}\,\sigma\, erf^{-1}(2P - 1). \qquad (4.1)$$

One can calculate a pixel value corresponding to a precision. Using an arbitrary precision of p=0,05 would mean 5% of the background would always be filtered. This value would also leave 5% of the background still visible after filtering. Using a 424x526 resolution this result in 11151 pixels still visible in the picture. Therefore when the drone is of size 300 pixels, this background would dominate all effects instead of the drone.

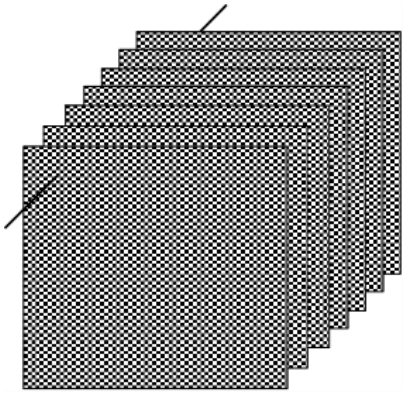

FIGURE 4.2 A GRAPHIC REPRESENTATION OF THE DATA. EACH LARGE SQUARE IS A FRAME CONTAINING 526X424 PIXELS OF DEPTH INFORMATION. EACH PIXEL HAS ITS OWN VARIANCE AND THEREFORE IN A STATIC VIDEO ONE CAN DETERMINE ITS STATISTICAL BEHAVIOR.

One might wonder why not make it approach zero? That would mean that nearly all pixels will always be filtered out and, therefore, also the foreground. Using a higher filter value means that close to the walls the filter could cut off the foreground which is undesirable. So finding the right value is important. Using information about the dimensions of the tunnel the reference camera area can be reduced to 300x270. Using an error margin of 1% on 300 pixels resulting in a filter value of p = 0,00005. When taking a closer look some pixels behave different ending up with a negative filter values. This would mean these points become blind spots, they never show the foreground. The reason for these 0 values is a pixel position alternating between two clearly different means. These blind spots could pose a problem, a short analysis shows they make up 1% of all pixels and are randomly distributed and are therefore negligible. Using the determined filter indeed results in high precision foreground images. Thereafter the filter can be used on real time image acquisition with around 15 fps giving full position information. The position is determined by some tedious Goniometrics on the pixel information. Using its relative angle and its field of view its position can be determined based on its average pixel depth and its average pixel position using formulas (4.2, 4.3, 4.4), with $\rho_{\alpha y}$ being the deviation in the pixel value from its center in y direction. And ρ_y being the pixel length of b. Where β and φ are its field of view in y and x direction respectively, and $\rho_{\alpha x}$ being its deviation from the middle for the x direction and ρ_x being the length of the x screen.

$$zpos = \sum_i^n pixel\_value \qquad (4.2)$$

$$ypos = h'' + d * \tan(\gamma + \frac{\rho_{\alpha y}}{\rho_y}\tan(\frac{\beta}{2})) \qquad (4.3)$$

$$xpos = \frac{\rho_{\alpha x}}{\rho_x}\tan(\frac{\varphi}{2}) * \sqrt{zpos^2 + ypos^2} \qquad (4.3)$$

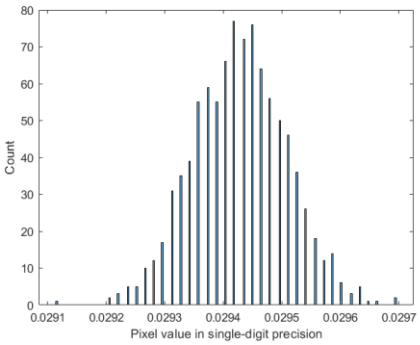

FIGURE 4.3 A HISTOGRAM OF AN ARBITRARY PIXEL ROW OF A BACKGROUND MEASUREMENT. IT IS CONVERTED FROM GREYSCALE TO SINGLE FOR STATISTICAL ANALYSIS.

FIGURE 4.4 AN ENHANCED ENLARGED VERSION OF OF THE DRONE USING A FILTERED FRAME P=0,00005. THE DRONE CONSISTS OF AT LEAST 99% OF THE NONZERO PIXELS IN THE FILTERED FRAME CALLED THE FOREGROUND IMAGE.

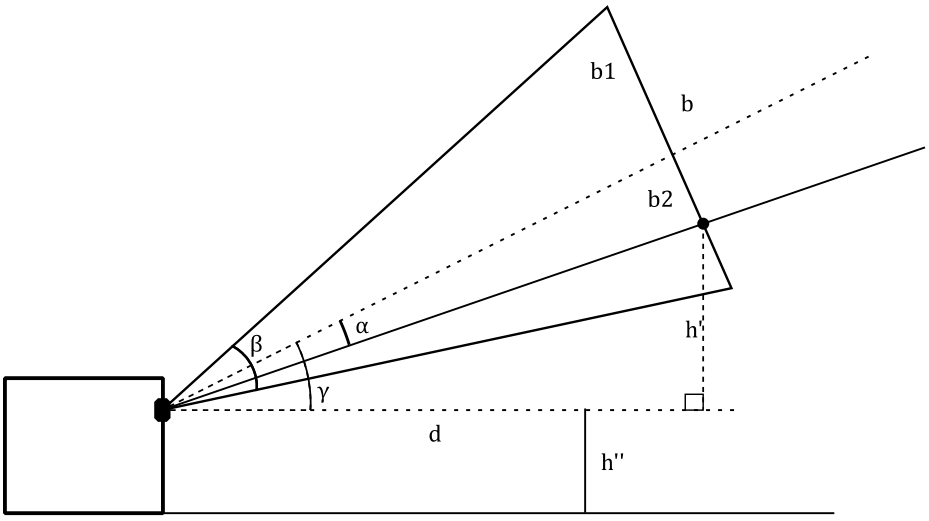

FIGURE 4.5 A SKETCH OF THE GEOMETRY OF THE KINECT IN 2D. SHOWING ALL ANGLES AND INFORMATION NEEDED TO CALCULATE THE Z AND Y POSITION OF THE DRONE. FOR X AN ADDITIONAL SKETCH IS REQUIRED.

4.3 Kinect and sunlight

During experimentation lines appeared on surfaces within the view of the camera. This is rather troublesome for the quality of the image acquisition. The origin for this phenomena is found to be sunlight, due to a change of background sunlight the reflective surfaces in the experimental setup reflected more or less light of the same wavelength of the Kinect tampering with the final image. This could also be the cause for some of the 2 peak behavior in the system mentioned before. Therefore use of the Kinect is best done indoor without observed exposure to sunlight.

4.4 Kinect precision

In order to investigate the quality of the Kinect a calibration measurement is done. The Kinect is suspended with relatively small wires such that these wires are invisible to the Kinect. The drones is positioned in a coordinate in the wind tunnel measured with a maximum standard error of about 2 centimeters shown in figure 4.6. Thereafter the drone is moved in the z direction changing its x-y coordinate

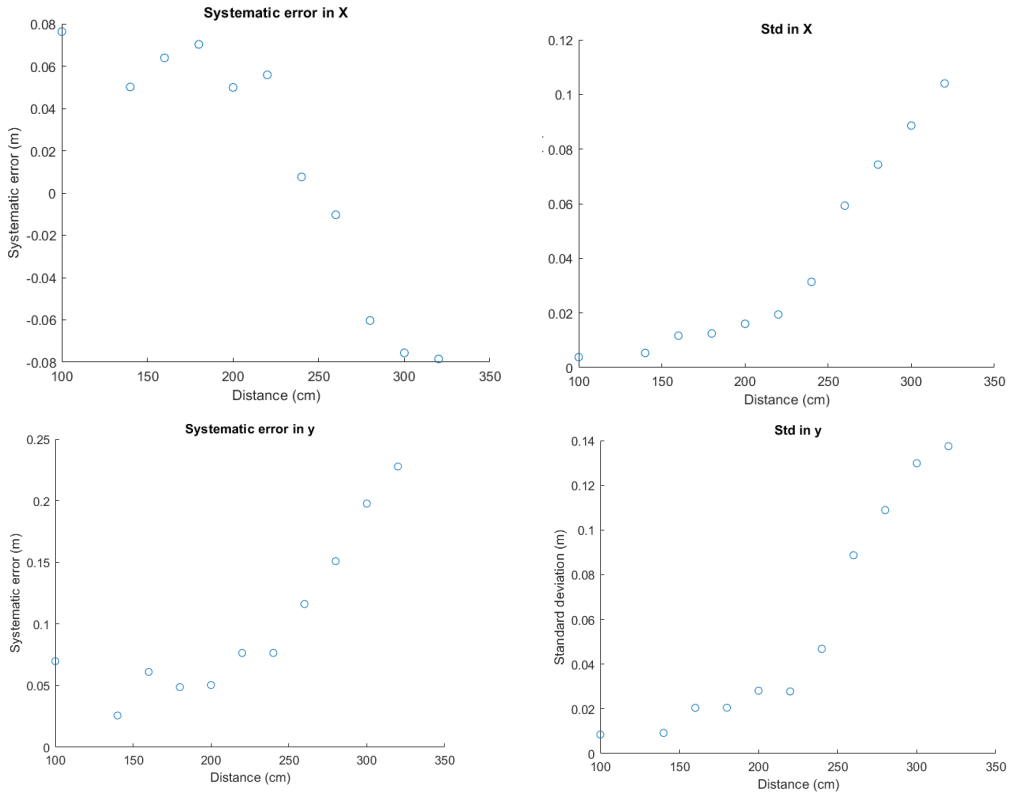

FIGURE 4.6 GRAPHS SHOWING THE PERFORMANCE OF THE KINECT SENSOR. WITH THE SYSTEMATIC ERROR BEING THE ERROR BETWEEN THE ACTUAL VALUE AND ITS MEASURED VALUE. ITS STANDARD DEVIATION IS DETERMINED AFTER TAKING A MULTITUDE OF MEASUREMENTS N=100.

as well as its total depth value. For each of this steps a multitude of filter values is used to show the impact of this value on its precision and bias. The Kinect has a position estimate that works best at close range due the size of the object being larger. In contrast to this statement the depth estimate has a small bias at short range but a better standard deviation.

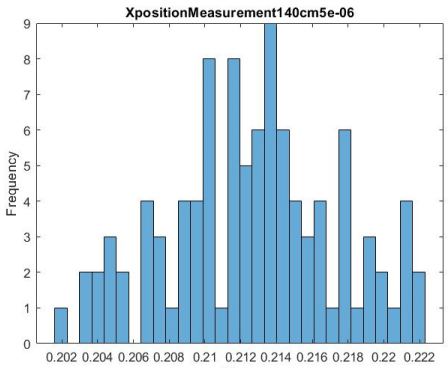

FIGURE 4.7 A HISTOGRAM OF THE MEASURED POSITION BY THE KINECT FOR A FILTER VALUE OF 5 E-6 AT A DISTANCE OF 140 CM. IT HAS A MEAN OF 0.212 WHICH IS CLOSE TO ITS REAL POSITION OF 0.208 (N=100).

Therefore its effectiveness is best on short distances and a representative pdf at 140cm is shown in figure 4.6. The standard deviation is per frame, and therefore averaging frames gives a group pdf according to basic summation of standard deviations, giving the option to improve on precision but losing refresh rate. Its statistical behavior is characterized in graph 4.6. Which concludes that the drone is able to locate the drone with a precision of about 2 centimeters when accounting for the current bias. And going beyond that when averaging over multiple frames.

5. Probability Density Functions

In order to measure the level of turbulence the principle of probability density functions is used. The drones PDF in different conditions are investigated in order to determine the accuracy of the acceleration sensor. Thereafter the pdf behavior of the suspended drone in turbulence is investigated.

5.1 Drone sensors

To explore the propellers influence on the sensor readings, a still and a high power measurement are made in figure 5.1a and 5.1b, respectively. When preforming the still measurement the limits of the sensor become apparent having a resolution size of magnitude $0.005\ m/s^2$. As expected, the standard deviation increases as the propellers start creating thrust. An unexpected behavior shows in the double peak behavior of figure 5.1a.

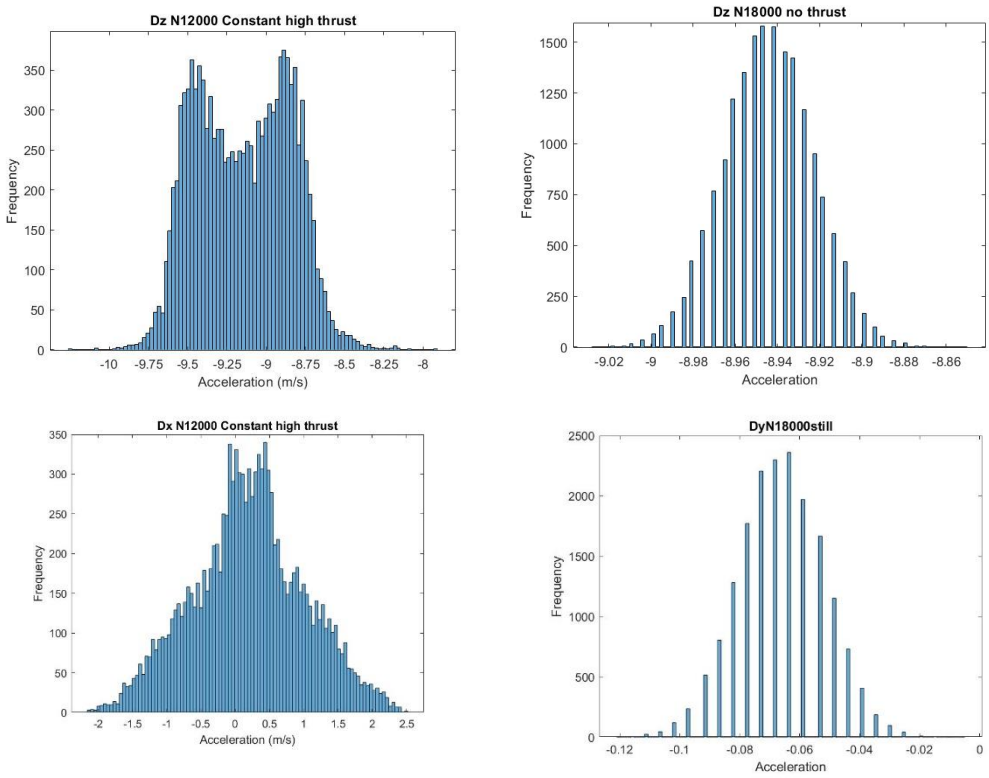

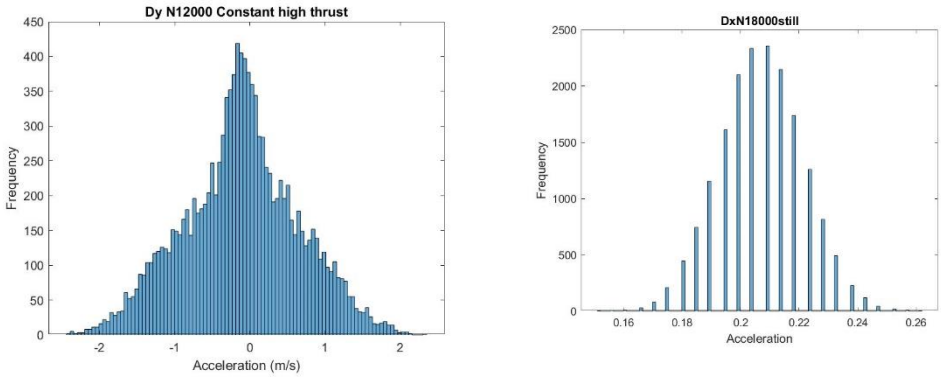

FIGURE 5.1 THE PROBABILITY DENSITY FUNCTIONS OF THE ACCELERATION IN THE Z, X AND Y DIRECTIONS WHEN THE DRONE IS HELD ON A FLAT SURFACE (ON THE LEFT SIDE, 5.1(A)) A DRONE USING HIGH THRUST N=12000 AND (ON THE RIGHT SIDE, 5.1(B)) USING NO THRUST N=18000.

This behavior was initially believed to be caused by the flight controller, but investigating further showed that this was not the case. The current and final assumption is that it is caused by the drone being fixed to the ground creating an oscillatory behavior. Having both the high powered measurement with and without the flight controller on a fixed drone the following standard deviation in x and y are roughly equal as suspected around 0.8 m/s^2 and due to vertical confinement the standard deviation in the z direction is better at 0.3 m/s^2. The double peak effect is clearly not helping its deviation. For the suspended measurements this is not an expected behavior. To confirm that this behavior is related to the way it is held down, suspended still and suspended thrust measurements are performed. These do not show the double peak but only a normal Gaussian which will be discussed in the next section.

5.2 Drone without Turbulence

In order to fully understand the drones behavior a multitude of measurements are performed. To finish the reference measurements of this work suspended measurements are performed, both still and using thrust, in order to determine the drones characteristics while suspended. Thereafter the drones' statistical properties are measured in different levels and types of flow, both turbulence and shear.

For these measurement the drone is suspended on top in the wind turbine according to figure 5.2. This method constraints its movement removing some information. The freedom in the x-y plane could contain enough information to answer our research question.

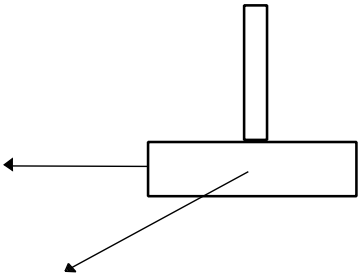

FIGURE 5.2 A SCHEMATIC DRAWING OF THE SUSPENSION OF THE DRONE. IT IS SUSPENDED ON TOP AND THEREFORE ITS Z DIRECTION IS CONSTRAINED INDEPENDENTLY FROM ITS ORIENTATION.

5.2.1 Reference measurements.

The reference measurements are reported here as a reference for following data. Using the statistics and graphs from this measurement it is possible to give meaning to the measurements in turbulence.

Firstly one of the important graphs is the unaltered raw data, for the still measurement it is not the most enticing graph, figure 5.3. It shows all the principal acceleration components and its absolute sum which should be equal to the acceleration due to gravity.

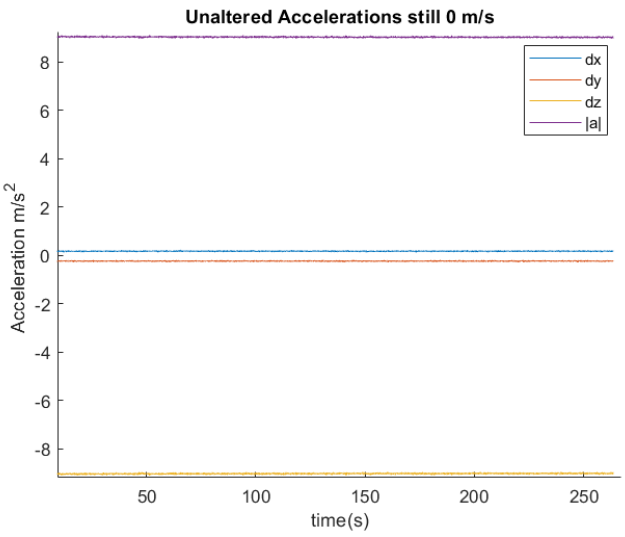

FIGURE 5.3 THE UNALTERED ACCELERATION SIGNAL OVER TIME OF A STILL SUSPENDED DRONE WITHOUT FLOW.

Our measurement approaches but are still off with a total of 9.0 m/s^2. In order to remove the effect of gravity each signal will be reduced by its own average or running average (We shall discuss the calculation of its running average later on). This makes each acceleration signal is now fluctuate around an average signal of approximately zero. Figure 5.4, reports the most essential information. The pdf of the absolute acceleration are reported in figure 5.4a, additionally their Fourier spectra are going to be discussed shown in figure 5.4b. These two figures hold most of the valuable information of the measurements because the pdf shows the statistical information and the Fourier transforms tells us about the frequency behavior.

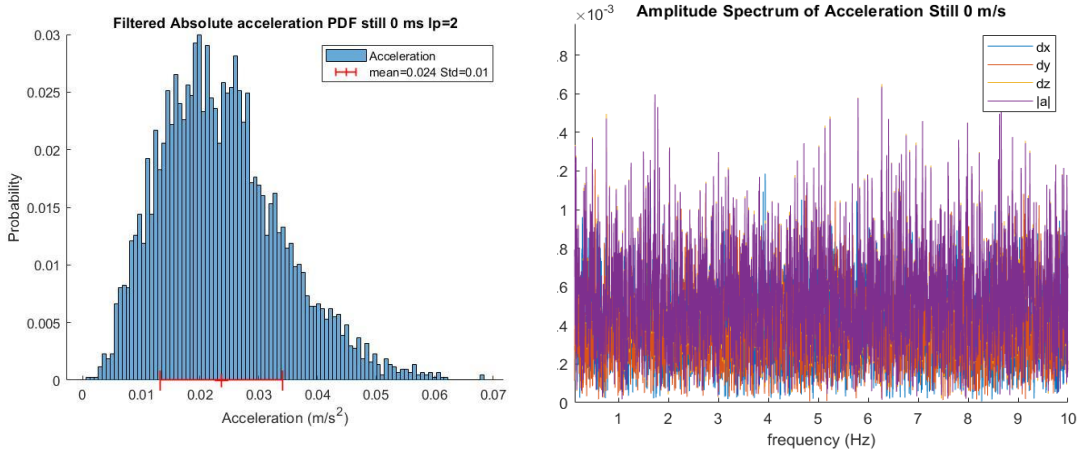

FIGURE 5.4 USING A STILL SUSPENDED DRONE WITHOUT FLOW. ON THE LEFT SIDE (A) THE ABSOLUTE ACCELERATION OF THE SIGNAL, CONTAINING INFORMATION FOR ALL ACCELERATION DIRECTIONS, ON THE RIGHT SIDE (B) THE FOURIER SPECTRUM OF A SIGNAL SHOWING NO FREQUENCIES ONLY NOISE.

Adding the mean and standard deviation in the form of an error bar to the pdf of the absolute acceleration the to show all important information at once, which now gives a baseline for all future data. The absolute acceleration is not Gaussian

even though each individual direction is normally distributed. The resulting distribution more resembles a Weibull distribution, this confirmation can be found in appendix A, assuming either Normal or Weibull distribution give the same mean and standard deviation. The amplitude spectrum shows that the sensor is finding noise of all frequencies with an average amplitude of roughly $0.0004\ m/s^2$.

We now report on acceleration measurements done by starting the drone and making the propellers turn at a speed approaching the lift-off thrust. This amount of thrust resembles the thrust it needs to levitate on its own. Having the drone suspended the following characteristics are shown in figure 5.5; the signal has significantly more noise and it also is now in motions as one can see in figure 5.5b. Using a low pass filter with a frequency of 0.01 Hz and a steepness(level of suppression) of 0.99 the low frequency movement of the drone is only visible. The relevance of these numbers will became apparent later on. For now it is important to see how it is indeed able to identify fluctuations with an amplitude of ~$0.5\ m/s^2$ from the original signal. This enables us to do only analysis on for example, low frequency signals or high frequency signals. The amplitude of the amplitude spectrum has increased significantly to about $0.03\ m/s^2$ on average and the mean of the absolute acceleration has become $1.7\ m/s^2$ with a standart deviation of $0.74\ m/s^2$. Both are around a magnitude of ~60 higher than its still counterpart.

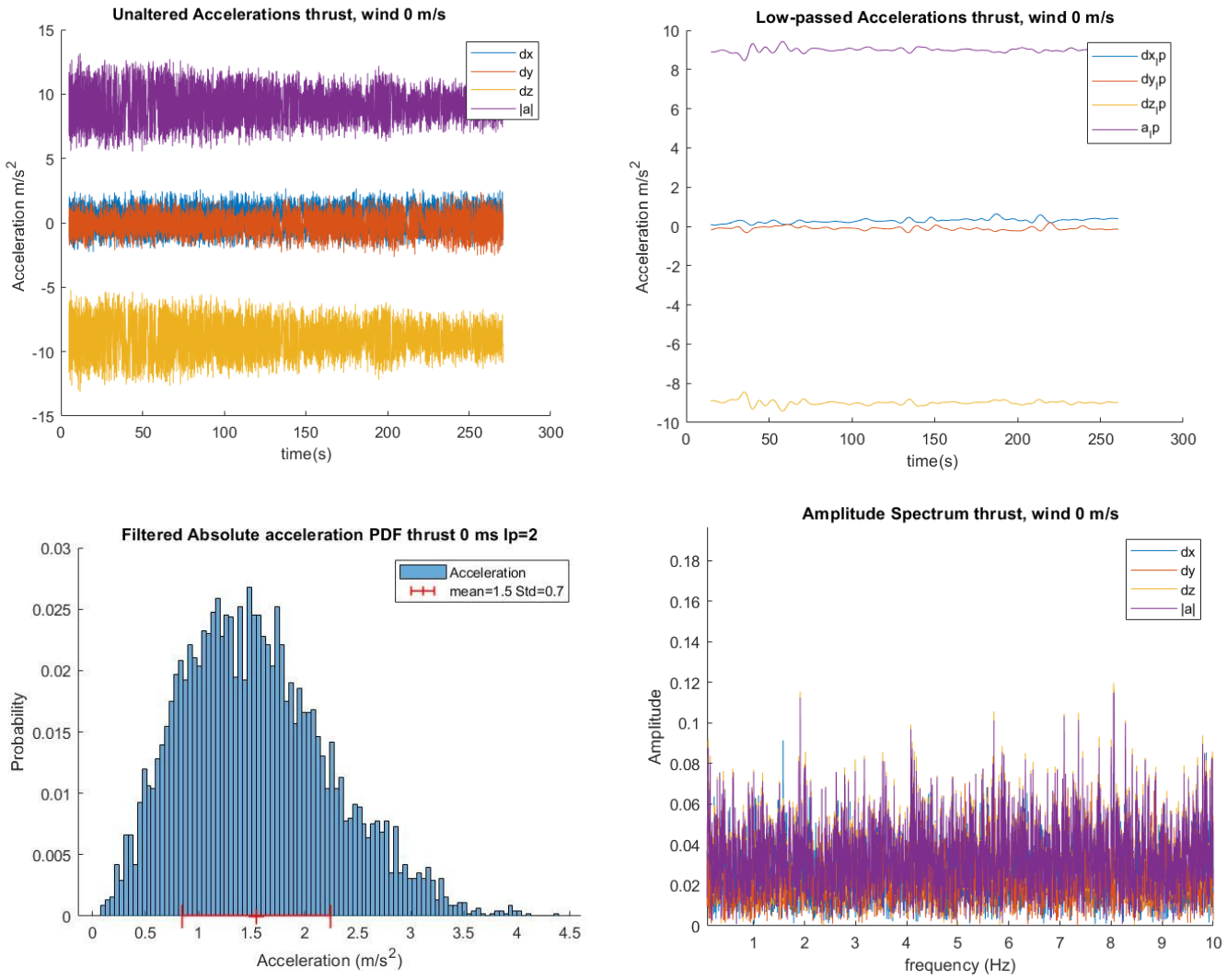

FIGURE 5.5 FOUR GRAPHS CHARACTERIZING THE BEHAVIOUR OF A SUSPENDED DRONE USING A CONTROLLER TO APPLY THRUST. ON THE TOP LEFT (A) THE RAW SIGNAL OF ITS ACCELEROMETER IS SHOWN. TOP RIGHT (B) THE LOW PASS FILTER IS SHOWN SHOWING THE SLOW ACCELERATION BEHAVIOR OF THE DRONE. BOTTOM LEFT (C) SHOWING THE ACCELERATION PDF AND ITS STATISTICS OF THE DRONE. BOTTOM RIGHT (D) SHOWS THE FOURIER SPECTRUM STILL NOT SHOWING AN CHARACTERISTIC FREQUENCIES.

5.2.2 Wind tunnel using laminar flow

In order to determine if the drone is influenced by turbulence another reference frame is needed. How does the drone behave when in laminar flow? Due to laminar flow having a constant velocity and the drone being suspended one of the possibilities is that it would find a point of equilibrium between gravitational and drag forces. Another possibility is finding a certain frequency on which the drone moves around an equilibrium being accelerated by the flow. In order to confirm or confute any of these hypothesis about the drone behavior, experimentally measurements are done.

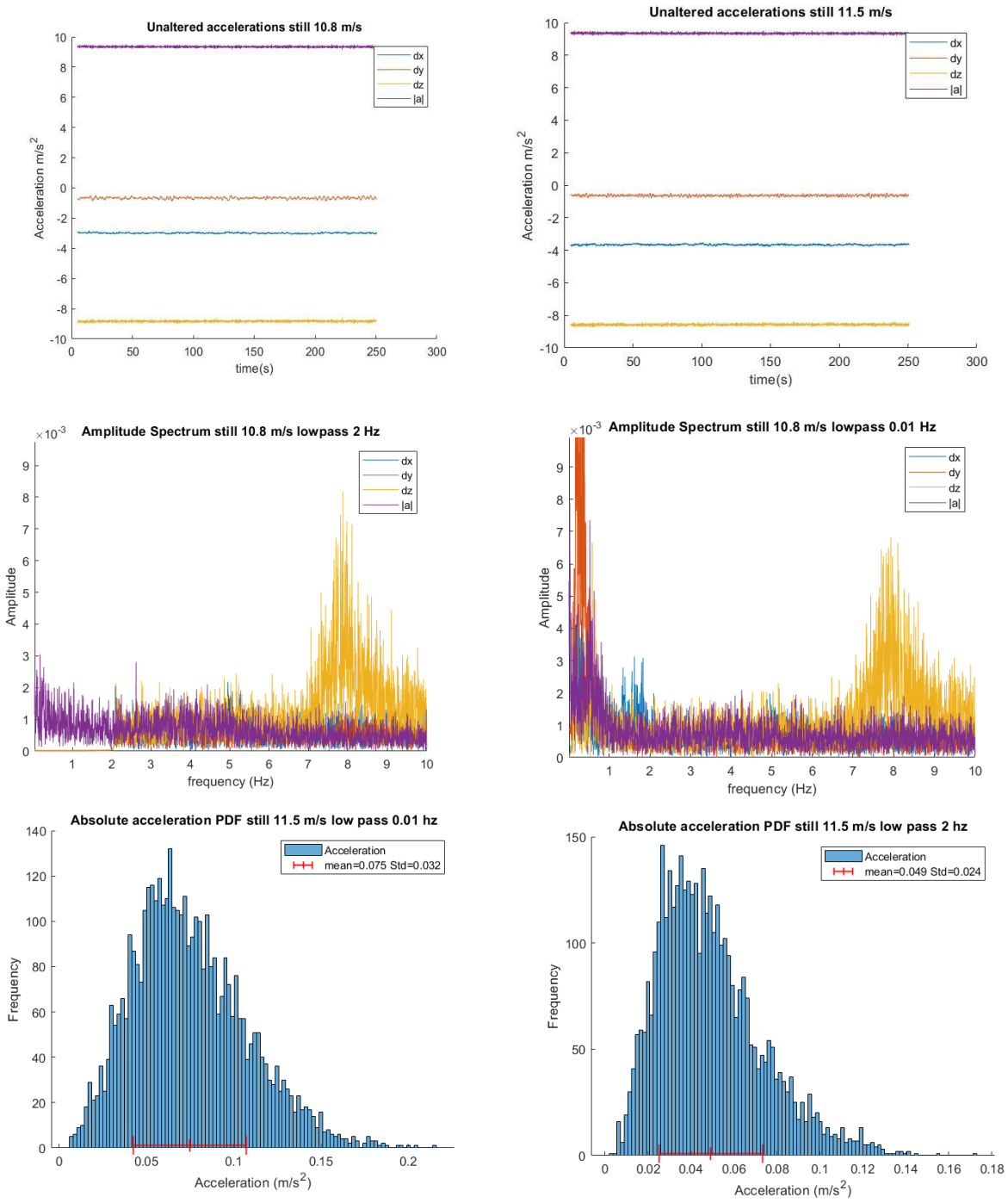

FIGURE 5.6 USING A SUSPENDED DRONE IN A LAMINAIR FLOW AT 10.8 AND 11.5 M/S. FOUR GRAPHS SHOWING THE EFFECT OF 2 DIFFERENT LOW PASS FILTERS ON ITS FREQUENCY SPECTRUM AND ITS ABSOLUTE ACCELERATION STATISTICS. (A) TOP LEFT, THE FILTERED AMPLITUDE SPECTRUM OF THE SAME MEASUREMENT AS ON THE TOP RIGHT ONLY USING A LOW PASS FREQUENCY OF 2HZ. (B) TOP RIGHT, A SIGNAL FILTERED USING A LOW PASS FREQUENCY VALUE OF 0.01 HZ, BOTTOM LEFT AND RIGH (C) AND (D) ARE THE ABSOLUTE ACCELERATION OF A DIFFERENT MEASUREMENT DEPICTING THE SAME BEHAVIOUR BUT ON ITS STATISTICS.

All the following measurements are done with the drone propellers removed as they would interfere with the measurement. The drone is suspended as before and the tunnel is creating a laminar flow. Using varying speeds the behavior of the wind tunnel and of the drone are characterized. Each flow speed has roughly the same pattern and behavior. To improve on its quality an important question arises, what frequencies are important? Varying flow speeds, the frequency region between 0 and 1 Hz shows periodic movement of the drone due to its suspension, this behavior does not scale proportional with flow speed, but rather if drone is able to stay in equilibrium. Therefore filtering this behavior from the data gives a stronger speed dependency. A filtered graph is shown in figure 5.6(a) the low frequency behavior is removed. A reduction in the absolute acceleration can be seen, which should reduce the noise in the calculation of the pdf. A frequency occurs at the 8 Hz domain in the z axis. But due to it only being in the z direction it does not impact on the absolute acceleration in a significant way. The corresponding PDF's are shown in in figure 5.6(c,d) showing the statistical properties and how the filter affects the PDF.

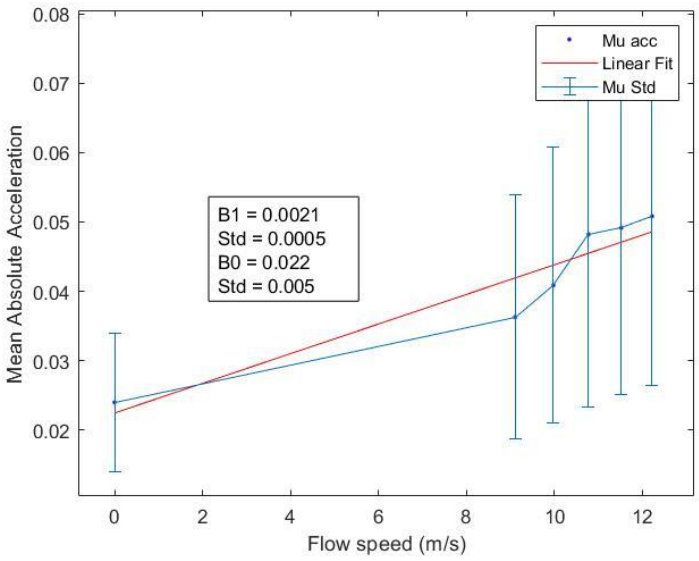

FIGURE 5.7 USING INCREASING FLOW SPEEDS IN LAMINAR FLOW, WHILE HAVING THE DRONE SUSPENDED, N=6500 PER DATAPOINT. SHOWING THE RELATIONSHIP BETWEEN THE AVERAGE ABSOLUTE ACCELERATION AND THE FLOW VELOCITY OF THE TUNNEL. WITH THE ERROR BARS BEING THE STANDART DEVIATION.

When relating flow speed and average absolute acceleration, the relation seems linear.

A different way of interpreting the data is by using the acceleration matrix formula (5.1), in table 5.1 it shows the flow is isotropic for the x and y directions. The z direction has a higher value since that direction is constrained and could be oscillating in its separate direction.

Matrix formula:

$$\sum_{i,j=1}^{3} a_i \cdot a_j = \begin{bmatrix} a_{ij} & \cdots & a_{zx} \\ \vdots & \ddots & \vdots \\ a_{xz} & \cdots & a_{zz} \end{bmatrix} \quad (5.1)$$

0.00054		
0.00055	0.00055	
0.00106	0.00107	0.00208

TABLE 5.1 SHOWING THE A MATRIC FOR THE LAMINAR FLOW AT 12.2 M/S N=6500, IN ITS AXIAL DIRECTION IT SHOWS THAT X AND Y ARE ISOTROPIC AND THAT Z IS NOT. THE MATRIX IS SYMMETRIC.

5.3 Drone in turbulence

Now having characterized the drone and the tunnel's characteristics, measurements in turbulence will be presented.

First the still drone will be measure at increasing flow speed, thereafter a second position further away from the passive grid, here the turbulence can be better developed. Lastly measurements using thrust are done in order to complete the data. For these measurements the drone is suspended in the same manner as used throughout the experiment, the grid used is one with a mesh size of 1 cm.

5.3.1 Initial location

The initial measurement location was 2 meters away from the grid. According to [5] this means a not yet fully developed turbulent flow. This position was used due to convenience and lack knowledge at the time of these measurements. Now with the introduction of turbulence the amplitude spectrum gets more interesting. Each spectrum showing the same behavior a peak around 6 Hz for all the directions shown in figure 5.8, it is found that the frequency of this peak changes based on the level of turbulence. The frequency behavior and the turbulence behavior for all measurements displayed in figure 5.9 by this it is clear the drone does measure some level of turbulence and is able to characterize its properties.

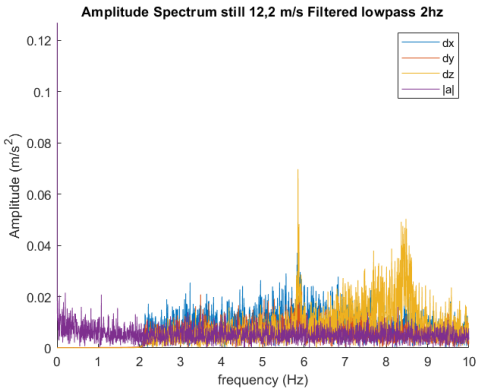

FIGURE 5.8 SHOWING THE FREQUENCY SPECTRUM OF THE DRONE IN TURBULENCE WHEN IT IS STILL, AT A SPEED OF 12.2 M/S

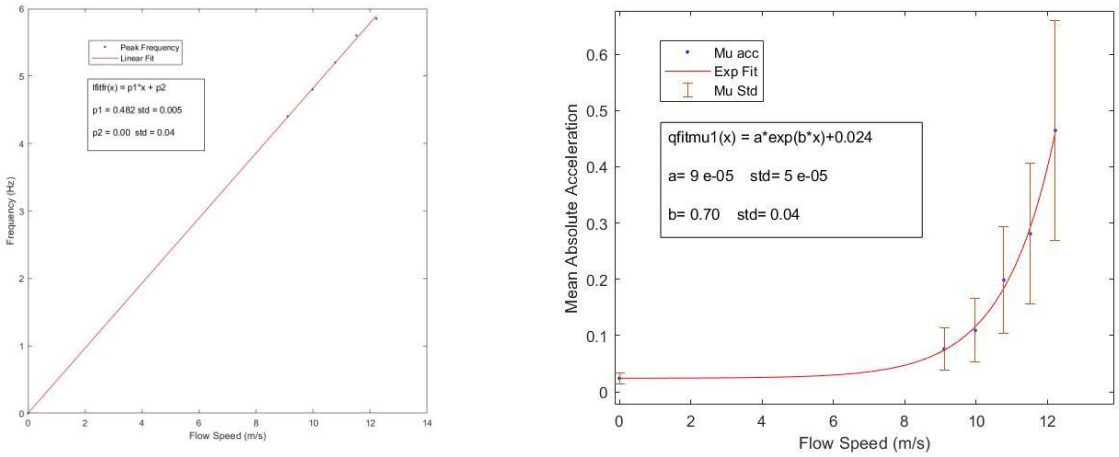

FIGURE 5.9 SUMMARIZING TURBULENCE STATISTICS AS A FUNCTION OF LOCATION. ON ITS RIGHT SIDE (B) THE ABSOLUTE ACCELERATION AS A FUNCTION OF FLOW SPEED AND ON ITS RIGHT Y AXIS ITS CHARACTERISTIC FREQUENCY AS A FUNCTION OF SPEED. N=6500 FOR ALL DATA POINTS.

5.3.2 Second location

To confirm the initial data another position in the tunnel is used, this position is 4.5 meters away from the grid which should mean the turbulence is more developed. This should result in higher absolute values but the same scaling. With 3 measurements frequency remains roughly the same on the higher frequencies in

contrast to the absolute acceleration which indeed increased in value. Its acceleration shows a more linear behavior which can be due to the small range of speed variation compared to the earlier measurement or the effects of propellers.

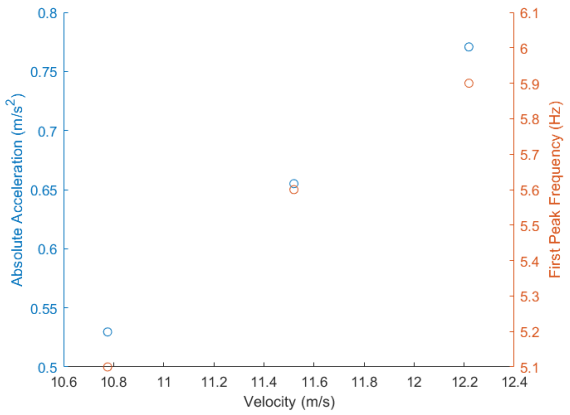

FIGURE 5.10 SHOWING THE TURBULENT BEHAVIORS AT A DISTANCE OF 4.5 M INSTEAD OF 2 M SHOWING HIGHER VALUES FOR THE ACCELERATION BUT THE SAME FREQUENCY BEHAVIOR. (N=6500)

5.3.3 Propellers

During still experimentation it occurred that when the flow reaches a critical speed the drone orientates so that its propellers start rotating. This rotation causes vibrations in the drone and therefore reduce its measuring properties. The Fourier analysis remains the same but its acceleration PDF clearly changes, shown in figure 5.11, therefore both measurements with propellers and without propellers will be done show how this effect is dominating other statistical properties.

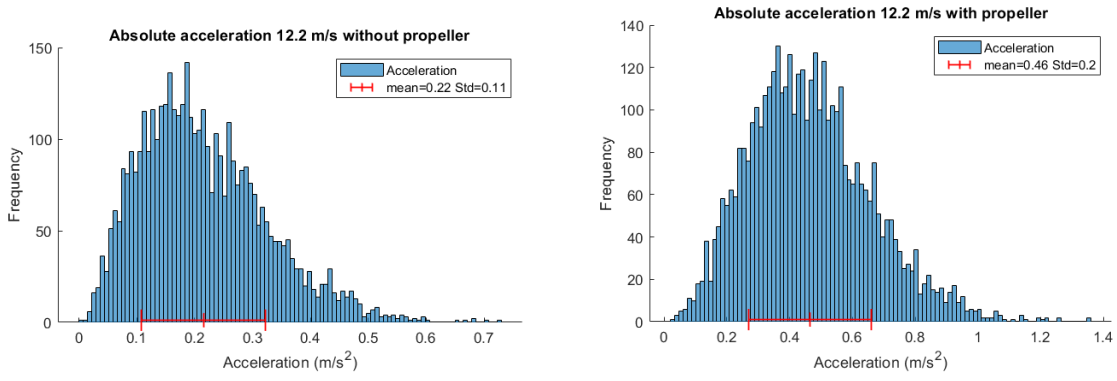

FIGURE 5.11 USING THE HANGING DRONE IN TURBULENT FLOW AT 12.2 M/S N=6500. TWO FIGURES SHOWING THE BEHAVIOR WITH THE LEFT SIDE WITHOUT PROPELLERS AND ON THE RIGHT SIDE WITH PROPELLERS.

5.3.4 Turbulence and thrust

A conclusive measurement is the drone actually interfering with turbulence by creating thrust. Earlier the background noise due to thrust has been characterized. 3 different set of measurements are done using thrust. Firstly on the 2 meter position data is acquired but showing no clear indication of any turbulence.

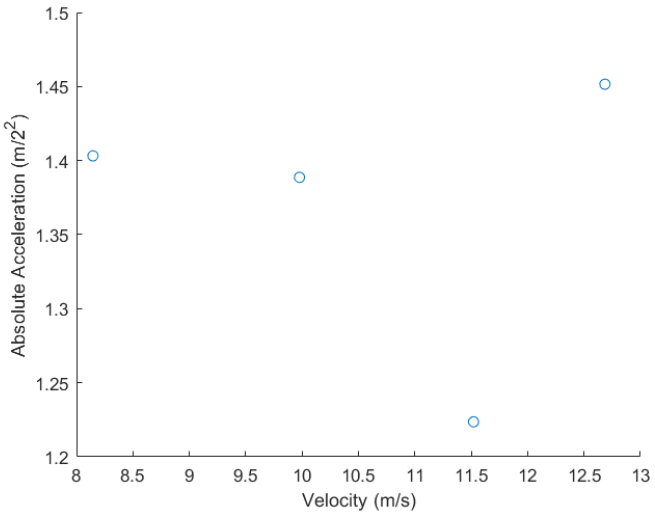

FIGURE 5.12 HAVING THE DRONE SUSPENDED IN INCREASING FLOW SPEED USING THE TURBULENCE GRID. SHOWING THE ABSOLUTE ACCELERATION PLOTTED AGAINST THE FLOW VELOCITY OF THE TUNNEL WHEN THE DRONE IS TRYING TO MAINTAIN CONSTANT THRUST WHILE USING THE CONTROLLER.

This is due to the fact that the actual flying of the drone has the same characteristics of the level of turbulence we are measuring, therefore when looking at PDFs no turbulence can be observed. To elaborate on the statistical properties table 5.2 relates the statistic for different types of measurements at a flow speed of 12.2 m/s. The average acceleration in laminar flow using the controller being higher than the average acceleration of the controller in turbulence is not entirely unexpected but still unwanted. Flying without any flow speed using manual controls, simulating a real flight scenario, results in an average of acceleration of 0.9 m/s^2 with a standard deviation of 0.4 m/s^2 assuming that flying higher flow speeds would result in more accelerations.

		Controller	Still
Turbulence	Average	0.9 m/s^2	0.8 m/s^2
	Std	0.4 m/s^2	0.4 m/s^2
Laminair	Average	1.3 m/s^2	0.05 m/s^2
	Std	0.4 m/s^2	0.03 m/s^2

TABLE 5.2 SUMMARIZING THE STATISTICAL INFORMATION FOR THE FLOW SPEED OF 12.2 M/S FOR DIFFERENT SITUATIONS ALTERING BETWEEN USING A CONTROLLER OR HAVE NO THRUST (STILL) AND USING LAMINAR OR TURBULENT FLOW.

Therefore only the amplitude spectrum remains an option to investigate turbulence while flying. Investigating this data for an extra measurement in the developed turbulent flow at 4.5m in a speed of 12.2 m/s the following spectrum is found figure 5.13. This data is rather strange due to its average amplitude being relatively low, its spectrum should look like the reference measurement figure 5.5(d) where the amplitude is relatively high all over the spectrum. The usual spectrum of a measurement in laminar flow using the controller have an amplitude of 0.2 m/s^2 around 6 Hz frequency which suggests in turbulence this peak could be measured which is supported by figure 5.13(a).

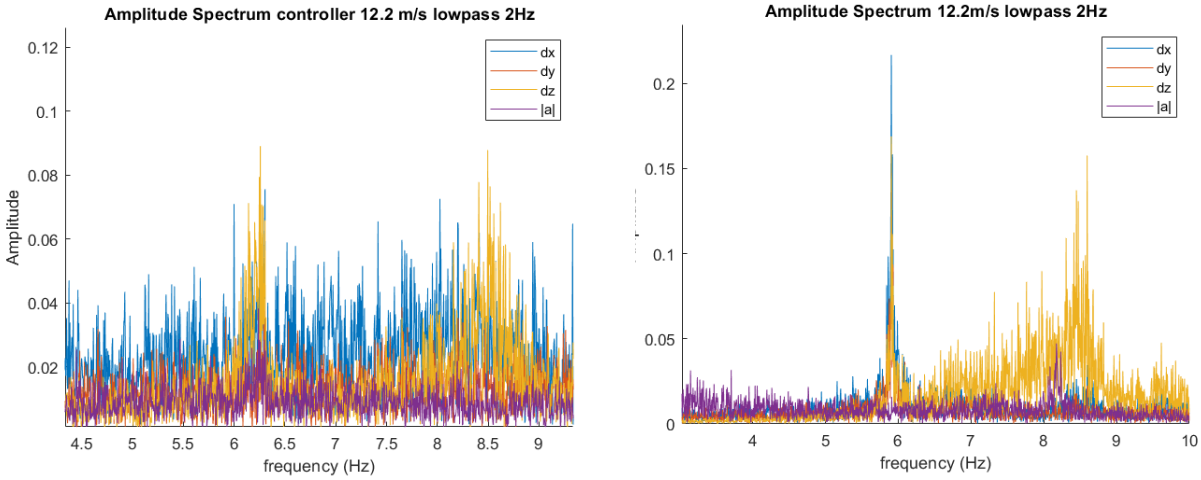

FIGURE 5.13 RELATING THE AMPLITUDE SPECTRUM OF TWO MEASUREMENTS DONE AT THE SAME SPEED OF 12.2 M/S AT 4.5. ON THE LEFT THE CONTROLLER IS RUNNING. ON THE RIGHT A STILL MEASUREMENT.

6. Conclusion

In order to answer the question of if a drone is able to measure turbulence, the drone's characteristics have been identified. Its accuracy in measuring gravitational acceleration at rest with a bias of $\sim 0.8\ \mathrm{m/s^2}$, but more importantly its standard deviation of $0.012\mathrm{m/s^2}$. Expectedly this accuracy increases when the drone comes in action, when its standard deviation with respect to acceleration increase to $0.4\mathrm{m/s^2}$. The drone's ability to measure is clearly limited by this error, therefore first a series of still measurements are done to quantify the effect of turbulence on a still drone. A clear linear relationship is found between frequency and flow speed. A non-linear relationship is found between flow speed and the absolute acceleration as seen in 5.9 and 5.10. These numbers have not been quantified towards any Reynolds numbers due to a lack of reference measurements on the turbulence. The absolute acceleration and a peak frequency varying from respectively $0{,}1 m/s^2$ to $0.9\mathrm{m/s^2}$ and 4,4 to 6,0 Hz. The origin of the absolute acceleration can be clearly defined as caused by turbulence. The frequency behavior could be a property of the suspended wire but this does not hold true due to it occurring in all 3 directions, also we cannot due to gravity. When the drone is flying and a low pass filter compensates for gravity and other low frequency fluctuations its absolute acceleration also becomes $0{,}9\ \mathrm{m/s^2}$ with an standard deviation of $0{,}4\ \mathrm{m/s^2}$. This means that the statistical information on flying are the same magnitude of the highest turbulence the wind tunnel could produce. Knowing that the absolute maximum flow speed the drone can take is 10 m/s compared to the turbulence measurement of 12.2 m/s it would never be able to measure that level of turbulence. Therefore it is impossible to do so with this drone. Another drone might be able to but it requires the absolute acceleration due to the propellers be lower than the acceleration of the turbulence.

Bibliography

[1] Chen, Ching Jen, Shenq- Yuh Jaw.(1998), Fundamentals of turbulence modeling. Taylor & Francis Washington Dc.

[2] Federico Toschi ,& Eberhard Bodenschatz (2008). Lagrangian Properties of Particles in Turbulence, Reviews in advance, doi:10.1146/annurev.fluid.010908.165210

[3] Roger Lewandowski, Benoît Pinier. The Kolmogorov Law of turbulence, What can rigorously be proved ? Part II. The Foundations of chaos revisited: from Poincaré to recent advancements, Springer, pp.71-89, 2016, 978-3-319-29699-9. ff10.1007/978-3-319-29701-9_5ff. ffhal-01244651f

[4] H.Tennekes,& J.L. Lumley (1972), A first course in turbulence, The Massachusetts Institute of Technology

[5] Hakkı Ergün Cekli (2011), How to stir turbulence, Universiteitsdrukkerij TU Eindhoven, Eindhoven, The Netherlands

[7] B.C.M. van Aert (2016), Control and Coordination Algorithms for Autonomous Multi-Agent Quadrotor Systems, Control Systems Technology Department of Mechanical Engineering Eindhoven University of Technology

[8] Cristopher T. Kilian (2001), Modern Control Technology Components and Systems 2nd edition, Delmar Thomson Learning

[9] L. Biferale, G. Boffetta, A. Celani, B. J. Devenish, A. Lanotte, & F. Toschi (2004), Multifractal Statistics of Lagrangian Velocity and Acceleration in Turbulence, Physical review letters Volume 93 number 6, DOI: 10.1103/PhysRevLett.93.064502

[10] By Robert Mahony,Vijay Kumar,& Peter Corke (2012), Multirotor Aerial Vehicles Modeling, estimation, and Control of Quadrotor, IEEE Robotics & automation magazine, DOI: 10.1109/MRA.2012.2206474.

[11] Parrot Drones SAS. https://www.parrot.com/nl/en/drones/parrot-mambo-fly

[13] A.R.P. Andri¨en, D. Antunes, M.J.G. van de Molengraft, W.P.M.H. Heemels ,Similarity-Based Adaptive Complementary Filter for IMU Fusion, unpublished.

Appendix A

Coding to verify distribution by looking at the plots and the residuals. The 3 suggested distributions are based on its original graph. The residual analysis is done on two separate magnitudes of binning. The binning is necessary because only unique values for its absolute accelerations are found. First a plot is made

```
%using matlabs fitting function for the 3 distributions.
dalpnorm = fitdist(ddalp,'Normal');
dalpgam = fitdist(double(ddalp),'Gamma');
dalpwei = fitdist(double(ddalp),'Weibull');

%the binning by rounding towards the nearest number
r3ddalp = round(ddalp,3);
r4ddalp = round(ddalp,4);

%using frequency table statistics to plot the graphs and later on calculating is
residuals.
freqinfo3=tabulate(r3ddalp);
freqinfo4=tabulate(r4ddalp);

%calculation of the pdf's based on the different distributions using the same
binning as the data.

y13= pdf(dalpnorm,freqinfo3(:,1,:));
y23= pdf(dalpgam,freqinfo3(:,1,:));
y33= pdf(dalpwei,freqinfo3(:,1,:));

y14= pdf(dalpnorm,freqinfo4(:,1,:));
y24= pdf(dalpgam,freqinfo4(:,1,:));
y34= pdf(dalpwei,freqinfo4(:,1,:));
```

```
%in the plot a normilazation based on the data is done the numbers are added
manually based on total sample number and its binning value.

figure
hold on
plot(freqinfo3(:,1,:),freqinfo3(:,2,:)/(4773*0.001))
plot(freqinfo3(:,1,:),y13)
plot(freqinfo3(:,1,:),y23)
plot(freqinfo3(:,1,:),y33)
legend('data','norm','gamma','weibull')
hold off

figure
hold on
plot(freqinfo4(:,1,:),freqinfo4(:,2,:)/(4773*0.0001))
plot(freqinfo4(:,1,:),y14)
plot(freqinfo4(:,1,:),y24)
plot(freqinfo4(:,1,:),y34)
legend('data','norm','gamma','weibull')
hold off

%finally calculation of the residuals based on its y coordinate.

resy13=sum(freqinfo3(:,2,:)/(4773*0.001)-y13)
resy23=sum(freqinfo3(:,2,:)/(4773*0.001)-y23)
resy33=sum(freqinfo3(:,2,:)/(4773*0.001)-y33)


resy14=sum(freqinfo4(:,2,:)/(4773*0.0001)-y14)
resy24=sum(freqinfo4(:,2,:)/(4773*0.0001)-y24)
```

resy34=sum(freqinfo4(:,2,:)/(4773*0.0001)-y34)

Resulting in the following graphs and data fig AppX. Based on the sum of residuals I conclude that the Weibull distribution is the right fit for the data.

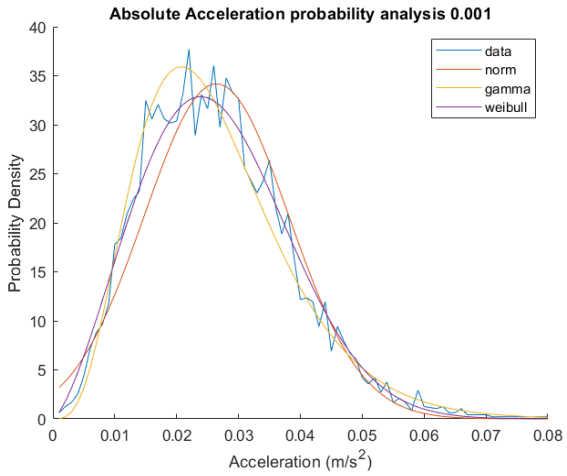

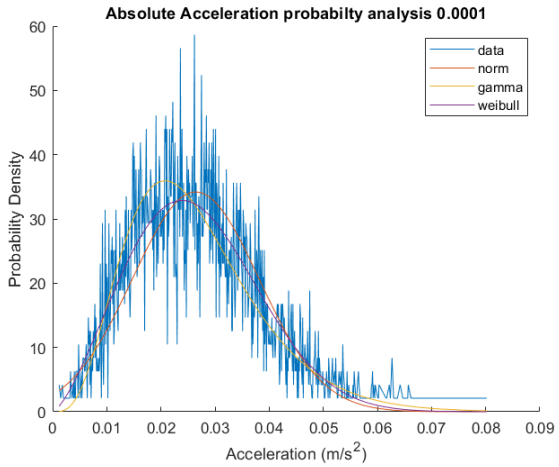

Sum of Residuals	0.001 binning	0.0001 binning
Normal	13.6	295.2
Gamma	4.5	227.1
Weibull	1.2	165.7